PHYSICAL REVIEW A VOLUME 18, NUMBER 5 NOVEMBER 1978

Elastic and pure rotational excitation of the hydrogen molecule by intermediate-energy electrons

P. K. Bhattacharyya
Department of Physics, Calcutta University, 92 Acharyya Prafulla Chandra Road, Calcutta 700009, India

K. K. Goswami
Department of Physics, Rishi Bankim Chandra College, Naihati, 24 Parganas, West Bengal, India

A. S. Ghosh*
Université de Bordeaux I, Laboratoire d'Astrophysique, 40, rue Lamartine, 33400 Talence, France
(Received 14 February 1978)

The eikonal amplitude for a fixed molecular orientation is used in the framework of the adiabatic approximation to calculate pure elastic excitation ($0\rightarrow0$ and $1\rightarrow1$), pure rotational excitation ($0\rightarrow2$ and $1\rightarrow3$), and average elastic cross sections of the hydrogen molecule in its ground electronic and vibrational states using electrons as incident projectiles. Both differential and integral cross sections are reported at electron energies 20–200 eV. For elastic processes, the effects of target polarization and electron exchange are considered, while for inelastic processes only the effect of the target polarization is taken into account. Results obtained are compared with those of other theoretical and experimental workers. It is found that pure elastic and pure rotational excitation cross sections are comparable at intermediate and large scattering angles, and that they depend on the initial rotational state J of the molecule in such a way that the average elastic cross sections remain independent of J.

I. INTRODUCTION

Recently[1] (Ref. 1 will hereafter be referred to as I) we presented a formulation for the study of the rotational excitation of homonuclear diatomic molecules initiated by the impact of electrons or positrons. This formulation is based on the adiabatic approximation in which the eikonal amplitude is used as the amplitude for a fixed molecular orientation. The eikonal amplitude and, as a consequence, different elastic and rotational excitation cross sections are expressed in terms of a highly converging series involving Bessel functions of increasing order. In I we reported our calculations for average (sum of pure elastic and rotational excitation) and pure rotational excitation ($1\rightarrow3$) cross sections for the e^--H_2 system at 40 eV. In the present paper we apply our theory to analyze in detail the problem of elastic and rotational excitation of hydrogen molecule by electron impact in the energy region 20–200 eV. We compute cross sections (both differential and total) for pure elastic ($0\rightarrow0$) and ($1\rightarrow1$), pure rotational ($0\rightarrow2$) and ($1\rightarrow3$), and also the average elastic processes. Earlier[2] we calculated the average cross sections using the scattering amplitude for three fixed molecular orientations. Obviously this procedure of averaging the molecular orientation is not reliable at large scattering angles for light molecules and almost all angles for heavy molecules, particularly at high energies, because of the dominance of nonspherical potential. Since this shortcoming is avoided in the present calculations we can expect better agreement with the experiment. It is well known[3] that the rotational excitations of molecules by electron impact are important at low energies and, in the past, the study of the rotational excitations of hydrogen molecules at low-energy region received considerable attention by both theorists and experimentalists. Recently Srivastava *et al.*[4] reported some experimental cross sections of hydrogen molecule for the process ($1\rightarrow3$) at electron energies 3–100 eV. These experimental cross sections showed some important features of the process. We examine these features in the light of our calculated cross sections. Apart from our preliminary calculations at 40 eV the only other theoretical studies of rotational excitation cross section ($1\rightarrow3$) reported so far are those of Truhlar *et al.*[5] and Truhlar and Brandt.[6] But these authors have considered the energy region 10–40 eV only. In a subsequent paper[7] we shall present our calculations for heavier molecular targets, nitrogen, and oxygen.

We give a brief outline of the theory in Sec. II. The potential models used in this paper are discussed in Sec. III. Results of our present calculations and their comparison with those of other theoretical and experimental workers are presented in Sec. IV. Finally, concluding remarks are given in Sec. V.

II. THEORY

We assume that the homonuclear diatomic molecule used as a target is in ground electronic and vibrational states so that the target may be treated as a rigid rotor. The incident electron of position vector $\vec{r}_3$ interacts with the target through the potential $V(\vec{r}_3,\hat{R})$, where $\hat{R}$ is the unit vector along the internuclear separation $\vec{R}$. Then the target wave functions are the spherical harmonics $Y_{JM}(\hat{R})$.

The adiabatic approximation is extensively used in nuclear and electron-molecule scattering problems.[3] The salient features of this approximation are as follows: if the incident electron velocity is quite high, the effective collision time is very much shorter than the period of molecular rotation and the collision problem can be considered as the scattering of electron by a molecular target whose axis is fixed in space. In such a condition the scattering amplitude obtained depends only on the internal coordinates of the target. The excitation cross sections are then derived by considering the change of the internal states of the molecule.

In the present situation the incident electron energies are very high and we make use of the adiabatic approximation. According to this approximation the differential cross section for the rotational excitation from the initial state J,M to the final state J',M' is given by[3] (we use atomic units throughout)

$$I(J,M\to J',M',\theta)=\left|\int Y^*_{J',M'}(\hat{R})f(\theta,\hat{R})Y_{JM}(\hat{R})\,d\hat{R}\right|^2. \tag{1}$$

On averaging over M and summing over M' we obtain the differential scattering cross section for the excitation process $(J\to J')$:

$$I(J\to J',\theta)=\frac{1}{2J+1}\sum_{M,M'}\left|\int Y^*_{J',M'}(\hat{R})f(\theta,\hat{R})Y_{JM}(\hat{R})\,d\hat{R}\right|^2. \tag{2}$$

The average elastic differential cross section is obtained by summing over J',M' and averaging over M in Eq. (1):

$$\langle I(\theta)\rangle=\frac{1}{4\pi}\int|f(\theta,\hat{R})|^2\,d\hat{R}, \tag{3}$$

where θ is the scattering angle and $f(\theta,\hat{R})$ is the scattering amplitude for a fixed orientation of $\vec{R}$.

We use eikonal amplitude for $f(\theta,\hat{R})$ which is given by

$$f(\theta,\hat{R})=-\frac{ik_i}{2\pi}\int e^{i\vec{q}\cdot\vec{b}_3}\times\left[\exp\left(-\frac{i}{v_i}\int_{-\infty}^{\infty}V(\vec{r}_3,\hat{R})\,dz_3\right)-1\right]d^2b_3, \tag{4}$$

with

$$\vec{r}_3=\vec{b}_3+\hat{k}_i z_3.$$

Here $m_e\vec{v}_i=\hbar\vec{k}_i$ is the incident electron's momentum and $q=\vec{k}_i-\vec{k}_f$ is the momentum transfer to the target. In the above expression the center of gravity is the origin and the direction of $\vec{k}_i$ is the polar axis. The electron-molecule interaction $V(\vec{r}_3,\hat{R})$ for a fixed internuclear separation R can be expanded in terms of Legendre polynomials

$$V(\vec{r}_3,\hat{R})=\sum_{\nu}V^{\nu}(r_3)P_{\nu}(\hat{r}_3\cdot\hat{R}), \tag{5}$$

with

$$\hat{r}_3\cdot\hat{R}=\cos\theta_3\cos\theta_m+\sin\theta_3\sin\theta_m\cos(\varphi_3-\varphi_m),$$

where θ_m,φ_m denote the orientation of the molecular axis with respect to the polar axis. For homonuclear diatomic molecules only the even values including zero for ν are allowed. We retain the first two nonvanishing terms $V^0(r_3)$ and $V^2(r_3)$. Using Eqs. (5) and (4) we get[1]

$$f(\theta,\hat{R})=-ik_i\sum_{n=0}i^n\lambda_n f_{2n,n}(\theta,\theta_m)\cos 2n\phi_m, \tag{6}$$

with

$$f_{2n,n}(\theta,\theta_m)=\begin{cases}\displaystyle\int_0^{\infty}J_0(qb_3)[e^{-i\chi(b_3,\theta_m)}\times J_0(\gamma)-1]b_3\,db_3, & \text{for } n=0,\\ \displaystyle\int_0^{\infty}e^{-i\chi(b_3,\theta_m)}\times J_{2n}(qb_3)J_n(\gamma)b_3\,db_3, & \text{for } n\neq 0,\end{cases}$$

$$\chi(b_3,\theta_m)=\frac{2}{v_i}\int_0^{\infty}V^0(r_3)\,dz_3+\frac{1}{v_i}(1-\tfrac{3}{2}\sin^2\theta_m)\times\int_0^{\infty}V^2(r_3)\frac{2z_3^2-b_3^2}{r_3^2}\,dz_3,$$

$$\gamma(b_3,\theta_m)=\frac{3}{2}\,\frac{\sin^2\theta_m}{v_i}\int_0^{\infty}V^2(r_3)\,\frac{b_3^2}{r_3^2}\,dz_3,$$

$$\lambda_n=\begin{cases}1, & \text{for } n=0,\\ 2, & \text{for } n\neq 0,\end{cases}$$

where J_n's are the Bessel functions of order n. Equations (6) and (2) yield the differential scattering cross section[8]

$$I(J\to J',\theta)=\frac{k_i^2(2J'+1)}{4}\sum_{M=-J}^{J}\left|\left(\frac{(J-|M|)!}{(J+|M|)!}\,\frac{(J'-|M'|)!}{(J'+|M'|)!}\right)^{1/2}\int P_J^{|M|}(\cos\theta_m)f_{2n,n}(\theta,\theta_m)\,P_{J'}^{|M'|}(\cos\theta_m)\sin\theta_m\,d\theta_m\right|^2, \tag{7}$$

where $2n=|M-M'|$. Average elastic differential cross section is obtained using Eq. (6) in Eq. (3):

$$\langle I(\theta)\rangle=\frac{k_i^2}{2}\sum_{n=0}\int\lambda_n f_{2n,n}^2(\theta,\theta_m)\sin\theta_m\,d\theta_m. \tag{8}$$

Total cross section $\sigma(J\to J')$ for the transition $J\to J'$ or the average total cross section $\langle\sigma\rangle$ are calculated using Eq. (7) or Eq. (8) in

$$\sigma=2\pi\int_0^\pi I\sin\theta\,d\theta. \tag{9}$$

We further define two other cross sections in the following way:

$$I_s(J,\theta)=I(J\to J,\theta)+I(J\to J+2,\theta), \tag{10}$$

and

$$\sigma_s(J)=\sigma(J\to J)+\sigma(J\to J+2). \tag{11}$$

It is to be noted that in $\langle I(\theta)\rangle$ and $\langle\sigma\rangle$ all the allowed final rotational states J' are included for any arbitrary initial state J while in $I_s(J,\theta)$ and $\sigma_s(J)$ only $J'=J+2$ is considered for a particular state J.

III. EFFECTIVE POTENTIAL

The eikonal amplitude, Eq. (6), is derived by taking the first two nonvanishing terms of the expansion given in Eq. (5). Of these the first term, $V^0(r_3)$, is spherically symmetric and the second term $V^2(r_3)$, is nonspherical and they are given by

$$V^0(r_3)=V_s^0(r_3)+V_{ex}^0(r_3)+V_p^0(r_3), \tag{12}$$

$$V^2(r_3)=V_s^2(r_3)+V_q^2(r_3)+V_p^2(r_3), \tag{13}$$

where V_s^0 and V_s^2 are the static potentials and V_q^2 is the long-range quadrupole tail of the static potential. V_s^0 and V_s^2 are obtained using simple H_2 wave function of Wang[9] (internuclear separation is taken to be $1.4a_0$) and are given in Ref. 2. We have replaced the effect of electron exchange by an effective local potential V_{ex}^0 due to Hara.[10] Since this exchange potential is spherically symmetric our inelastic cross sections do not take into account the effect of electron exchange. V_p^0 and V_p^2 are, respectively, the spherical and nonspherical parts of the polarization potential. The long-range potentials V_q^2, V_p^0, and V_p^2 have the asymptotic form

$$V(r_3)\xrightarrow{r_3\to\infty}\frac{Q}{r_3^3}-\frac{\alpha_0}{2r_3^4}-\frac{\alpha_2}{2r_3^4}, \tag{14}$$

where Q is the quadrupole moment of the molecule. α_0 and α_2 are respectively, the spherical and nonspherical parts of the static dipole polarizability. The small-r_3 behavior of these long-range potentials are not adequately known. These potentials are usually approximated by introducing suitable cutoff parameters which eliminate the singularity at the gravity center of the molecule as well as give proper fit to the experimental cross sections. In the present investigation we use two forms for $V_q^2(r_3)$, $V_p^0(r_3)$, and $V_p^2(r_3)$:

Model A

$$V_q^2(r_3)=-Qr_3^3(r_3^2+R_0^2)^{-3},\quad V_p^0(r_3)=-\tfrac{1}{2}\alpha_0(r_3^2+R_0^2)^{-2},$$

$$V_p^2(r_3)=-\tfrac{1}{2}\alpha_2 r_3^2(r_3^2+R_0^2)^{-3},$$

where the cutoff parameter R_0 is taken to be equal to $1.6a_0$;

Model B

$$V_q^2(r_3)=-Qr_3^{-3}(1-e^{-(r_3/r_0)^6}),$$

$$V_p^0(r_3)=-\tfrac{1}{2}\alpha_0(r_3^2+R_1^2)^{-2}(1-e^{-(r_3/R_a)^3}),$$

$$V_p^2(r_3)=\begin{cases}0, & r_3<0.5a_0,\\ -\tfrac{1}{2}\alpha_2(r_3^2-R_2^2)^{-2}(1-e^{-(r_3/R_b)^4}), & r_3\geq 0.5a_0,\end{cases}$$

where $R_1=1.22a_0$, $R_2=0.1a_0$, $R_a=1.7a_0$, $R_b=2.0a_0$, and $r_0=1.8a_0$. In both the models, Q, α_0, and α_2 are taken to be $0.490e^2a_0^2$, $5.1786e^2a_0^2$, and $1.2019e^2a_0^3$, respectively. The parameter in model A was given by Hara[10] while the parameters in model B were determined by Henry and Lane.[11]

IV. RESULTS AND DISCUSSIONS

A. Numerical integration and cross sections

The two-dimensional integration in Eqs. (7) and (8) and z_3 integration in $\chi(b_3,\theta_m)$ and $\gamma(b_3,\theta_m)$ are performed numerically. In case of b_3 and z_3 integration the integrated range is divided into a number of meshes (80 to 120 for b_3 and 50 to 70 for z_3 depending on energy) with variable step sizes and eight-point Gauss-Legendre quadrature is used for

the integration of each mesh. The angular integration from $\theta_m = 0$ to $\theta_m = 90°$ is performed using eight-point Gauss-Legendre quadrature. For the average elastic differential cross section, Eq. (8), only first three terms are found to give well-convergent results throughout the energy range considered.

Differential and total cross sections are calculated for the elastic processes $(0 \rightarrow 0)$ and $(1 \rightarrow 1)$ with and without exchange and for the rotational excitation processes $(0 \rightarrow 2)$ and $(1 \rightarrow 3)$ neglecting exchange at energies between 20 and 200 eV. Both the potential models A and B are considered in these calculations. Average elastic differential cross sections using Eq. (8) and average total cross sections using Eqs. (8) and (9) are also obtained. In Figs. 1–3 the differential cross sections for some of the processes are plotted against the scattering angles at and below 100 eV. Average elastic cross sections are compared with the experimental results of different workers in Figs. 6–9. The differential cross sections for all the elastic and inelastic processes mentioned above and the average elastic differential cross sections at 30, 40, and 50 eV are given in Tables I–III. Total cross sections and momentum transfer cross sections at 20–200 eV are shown in Tables IV and V, respectively.

B. Pure elastic and rotational excitation cross sections and ratios

In Fig. 1 the differential cross sections for the processes $(1 \rightarrow 1)$ and $(1 \rightarrow 3)$ at 40 eV are compared with the corresponding experimental[4] and theoretical[5,6] quantities. We use the experimental elastic $(1 \rightarrow 1)$ cross sections of Srivastava *et al.*[4] as tabulated in Ref. 5. These cross sections are in good agreement with our calculated cross section (with exchange). The agreement is better for the model B. The inelastic $(1 \rightarrow 3)$ cross sections obtained using the potential model B are higher at small and intermediate scattering angles than those for model A but they show completely opposite angular dependence in the two models. Cross sections for model A show a minimum at about 25° while those for model B give a maxima around 50°. For both the models the calculated cross sections underestimate the experimental cross sections of Srivastava *et al.* but surprisingly the potential model A reproduces correctly the angular dependence found experimentally.

The general features of the inelastic $(1 \rightarrow 3)$ differential scattering cross sections at 40 eV for potential models A and B discussed above are found to represent typically those of the rotational $(1 \rightarrow 3)$ cross sections (Fig. 2) and $(0 \rightarrow 2)$ cross sections

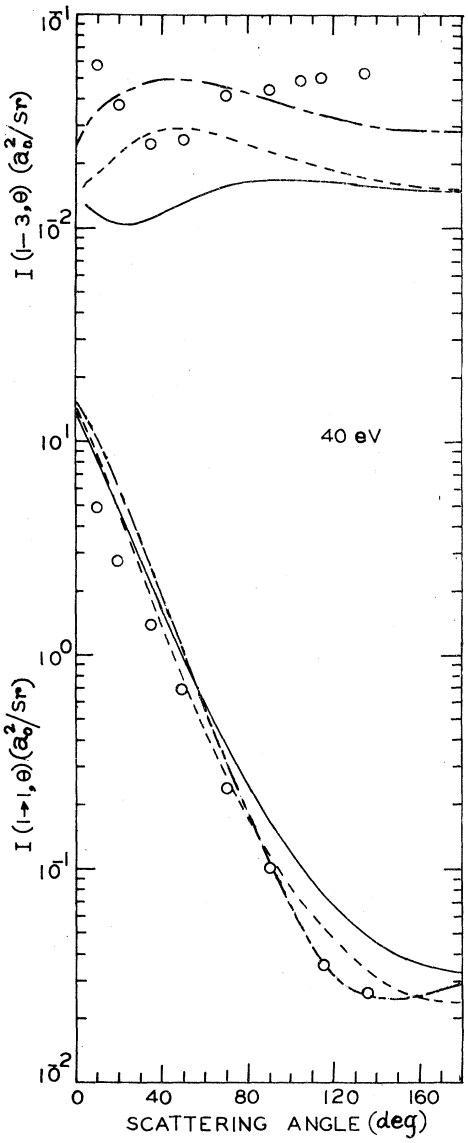

FIG. 1. Differential cross sections as a function of scattering angles at 40 eV: (i) Lower curves for elastic transition $J = 1 \rightarrow J' = 1$: dash-dotted line, Ref. 6 (potential model 3); straight line, model A and dashed line, model B, present calculations with exchange; (ii) Upper curves for inelastic transition $J = 1 \rightarrow J' = 3$: dashed-dotted line, Ref. 6 (potential model 3XE); straight line, model A and dashed line, model B, present calculations without exchange. Open circles are the experimental results of Ref. 4 as reported in Ref. 5.

(Fig. 3) at different energies. At each energy $(0 \rightarrow 2)$ cross sections are higher than $(1 \rightarrow 3)$ cross sections but the minimum in model A or the maximum in model B occurs at the same angle for the two processes. These angles decrease with the in-

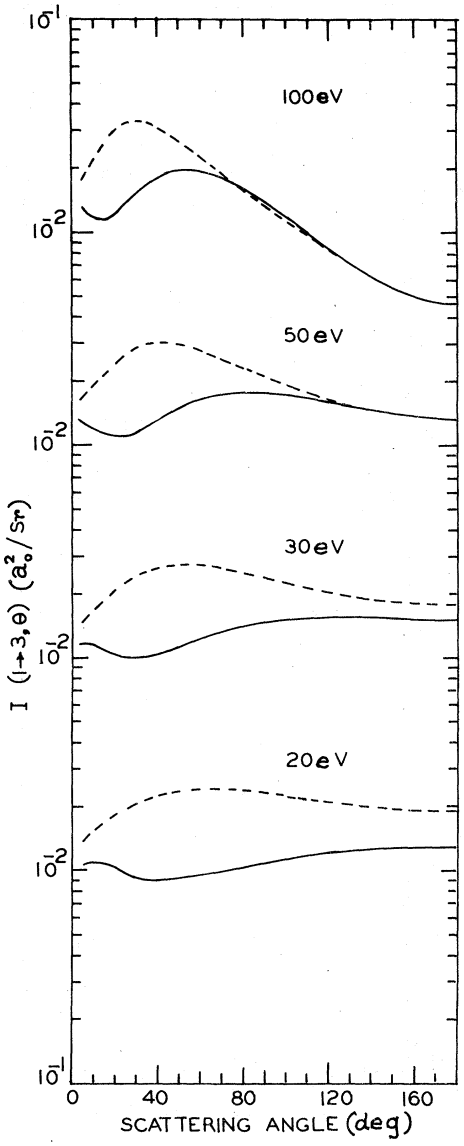

FIG. 2. Rotational-excitation differential cross section for the transition $J=1 \rightarrow J'=3$. Solid and broken curves are present results for potential models A and B, respectively.

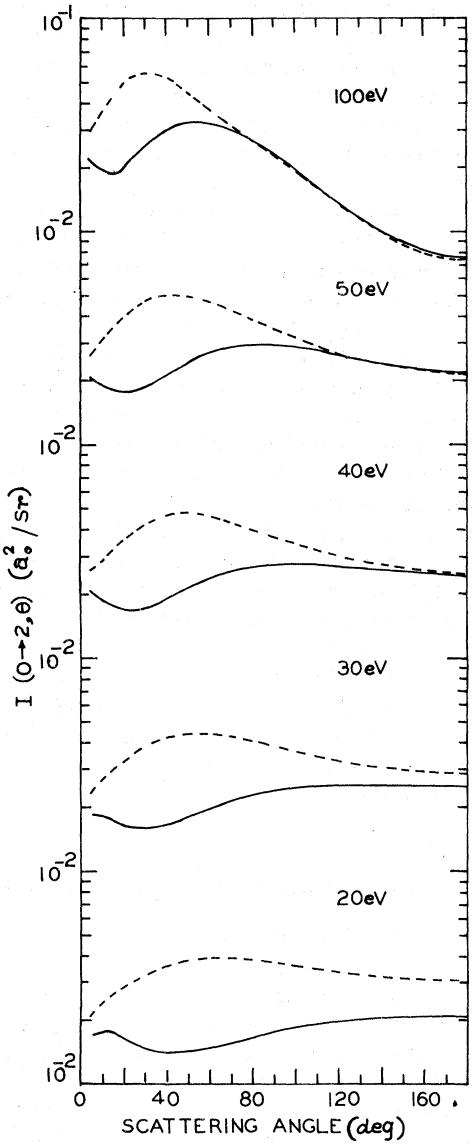

FIG. 3. Rotational-excitation differential cross sections for the transition $J=0 \rightarrow J'=2$. Solid and broken curves are present results for potential models A and B, respectively.

crease in energy. The inelastic differential cross sections are found to decrease very sharply at or near the forward direction. It is not unexpected since the Glauber-type eikonal approximation is in principle not valid for small angle inelastic scattering.[12] From Tables I–IV it is interesting to note that the pure elastic, $I(J \rightarrow J, \theta)$ and $\sigma(J \rightarrow J)$, and inelastic $I(J \rightarrow J+2, \theta)$ and $\sigma(J \rightarrow J+2)$, cross sections depend upon the initial rotational state J. With the increase in J cross sections increase for elastic processes while they decrease for inelastic processes in such a way that $I_s(J, \theta)$ and $\sigma_s(J)$ remain insensitive to initial rotational state J. Furthermore, $I_s(J, \theta)$ and $\sigma_s(J)$ are found to be equal to the corresponding average cross sections $\langle I(\theta) \rangle$ and $\langle \sigma \rangle$. It shows that contribution of higher-order inelastic cross sections is negligible in the energy region considered here. Dependence of pure elastic and inelastic processes on J and the insensitivity of total cross sections on J were also found in low-energy e-H_2 scattering.[13]

TABLE I. Differential cross sections (a_0^2/sr) at 30 eV.

(deg)	Model	$I(0\rightarrow0)$ $\times10^{-2}$	$I(0\rightarrow0)$ [a] $\times10^{-2}$	$I(0\rightarrow2)$ $\times10^{-2}$	$I(1\rightarrow1)$ $\times10^{-2}$	$I(1\rightarrow1)$ [a] $\times10^{-2}$	$I(1\rightarrow3)$ $\times10^{-2}$	$\langle I\rangle$ $\times10^{-2}$	$\langle I\rangle^a$ $\times10^{-2}$
0	A	1167	1311	0.608	1167	1311	0.410	1168	1312
	B	1230	1405	0.960	1231	1406	0.639	1231	1407
10	A	694.6	811.1	1.866	695.4	811.9	1.164	696.6	813.1
	B	721.0	859.5	2.716	722.1	860.6	1.169	723.9	862.4
20	A	416.0	501.9	1.669	416.6	502.5	1.046	417.7	503.6
	B	410.2	509.9	3.278	411.5	511.2	2.028	413.6	513.2
30	A	254.6	313.9	1.600	255.3	314.5	1.003	256.3	315.6
	B	233.0	300.1	3.823	234.5	301.5	2.353	237.0	303.8
40	A	158.2	197.3	1.659	158.8	197.9	1.036	159.9	199.0
	B	132.8	176.1	4.239	134.5	177.6	2.600	137.2	180.3
50	A	99.64	125.2	1.811	100.4	125.9	1.125	101.5	127.0
	B	76.89	104.4	4.475	78.68	106.0	2.738	81.49	109.6
60	A	64.04	80.96	1.976	64.83	81.69	1.221	66.09	82.95
	B	45.87	63.61	4.474	47.66	65.24	2.734	50.46	67.97
70	A	42.16	53.80	2.144	43.01	54.59	1.320	44.38	55.93
	B	28.46	40.29	4.343	30.20	41.87	2.652	32.91	44.65
80	A	28.54	36.95	2.294	29.46	37.78	1.408	30.91	39.30
	B	18.45	26.67	4.145	20.11	28.18	2.530	22.69	30.86
90	A	19.93	26.29	2.410	20.90	27.16	1.475	22.41	28.74
	B	12.48	18.43	3.927	14.05	19.88	2.396	16.50	22.34
100	A	14.38	19.38	2.490	15.37	20.28	1.521	16.93	21.88
	B	8.791	13.25	3.714	10.28	14.64	2.266	12.59	16.94
110	A	10.73	14.78	2.531	11.74	15.71	1.544	13.32	17.36
	B	6.429	9.883	3.514	7.834	11.21	2.144	10.03	13.39
120	A	8.278	11.66	2.550	9.298	12.60	1.555	10.88	14.21
	B	4.874	7.633	3.346	6.213	8.915	2.041	8.300	10.98
140	A	5.498	8.048	2.550	6.518	8.999	1.552	8.099	10.58
	B	3.136	5.071	3.101	4.376	6.280	1.892	6.310	8.176
160	A	4.271	6.414	2.532	5.284	7.364	1.540	6.852	8.947
	B	2.380	3.935	2.964	3.566	5.102	1.808	5.414	6.920
180	A	3.918	5.935	2.520	4.926	6.883	1.532	6.485	8.453
	B	2.165	3.606	2.913	3.330	4.757	1.777	5.146	6.551

[a] With exchange. $\langle I\rangle^a$ does not include the effect of exchange on rotational-excitation cross sections.

TABLE II. Differential cross sections (a_0^2/sr) at 40 eV.

(deg)	Model	$I(0\rightarrow0)$ $\times10^{-2}$	$I(0\rightarrow0)$ [a] $\times10^{-2}$	$I(0\rightarrow2)$ $\times10^{-2}$	$I(1\rightarrow1)$ $\times10^{-2}$	$I(1\rightarrow1)$ [a] $\times10^{-2}$	$I(1\rightarrow3)$ $\times10^{-2}$	$\langle I\rangle$ $\times10^{-2}$	$\langle I\rangle^a$ $\times10^{-2}$
0	A	1247	1400	0.567	1247	1400	0.378	1248	1400
	B	1293	1469	0.854	1293	1470	0.567	1294	1470
10	A	693.0	809.9	1.870	693.7	810.7	1.160	694.9	811.9
	B	701.0	833.2	2.851	702.2	834.4	1.764	704.0	836.2
20	A	389.4	470.4	1.718	390.1	471.1	1.068	391.2	472.2
	B	367.9	456.6	3.628	369.4	458.1	2.228	371.7	460.3
30	A	223.2	275.3	1.730	223.9	276.0	1.073	225.0	277.1
	B	192.0	247.1	4.291	193.7	248.9	2.623	196.4	251.3
40	A	129.2	161.4	1.903	130.0	162.1	1.174	131.2	163.3
	B	100.4	133.1	4.715	102.3	134.9	2.874	105.3	137.7
50	A	75.73	95.37	2.154	76.59	96.18	1.323	77.95	97.56
	B	53.62	72.88	4.837	55.56	74.70	2.943	58.55	77.71
60	A	45.28	57.55	2.376	46.22	58.44	1.453	47.72	59.94
	B	29.77	41.37	4.659	31.63	43.13	2.833	34.52	46.03
70	A	27.73	35.74	2.568	28.76	36.70	1.565	30.36	38.30
	B	17.30	24.57	4.373	19.06	26.22	2.658	21.76	28.98
80	A	17.49	22.95	2.705	18.57	23.97	1.646	20.24	25.64
	B	10.53	15.28	4.059	12.16	16.83	2.467	14.67	19.34

TABLE II (*Continued*)

(deg)	Model	$I(0\rightarrow 0)$ $\times 10^{-2}$	$I(0\rightarrow 0)^a$ $\times 10^{-2}$	$I(0\rightarrow 2)$ $\times 10^{-2}$	$I(1\rightarrow 1)$ $\times 10^{-2}$	$I(1\rightarrow 1)^a$ $\times 10^{-2}$	$I(1\rightarrow 3)$ $\times 10^{-2}$	$\langle I\rangle$ $\times 10^{-2}$	$\langle I\rangle^a$ $\times 10^{-2}$
90	A	11.38	15.28	2.776	12.49	16.33	1.686	14.20	18.05
	B	6.695	9.920	3.755	8.197	11.37	2.282	10.52	13.67
100	A	7.658	10.55	2.792	8.775	11.61	1.694	10.49	13.34
	B	4.416	6.686	3.484	5.810	8.045	2.117	7.962	10.18
110	A	5.337	7.550	2.769	6.445	8.607	1.679	8.147	10.32
	B	3.018	4.671	3.252	4.318	5.952	1.976	6.327	7.931
120	A	3.863	5.611	2.725	4.953	6.658	1.652	6.627	8.336
	B	2.139	3.385	3.062	3.363	4.601	1.861	5.256	6.481
140	A	2.298	3.497	2.607	3.341	4.508	1.579	4.940	6.106
	B	1.217	2.011	2.775	2.327	3.126	1.687	4.043	4.849
160	A	1.660	2.608	2.514	2.666	3.589	1.522	4.208	5.124
	B	0.848	1.448	2.611	1.892	2.506	1.587	3.507	4.132
180	A	1.485	2.358	2.478	2.476	3.327	1.500	3.995	4.837
	B	0.748	1.294	2.554	1.769	2.326	1.552	3.349	3.923

[a] With exchange. $\langle I\rangle^a$ does not include the effect of exchange on rotational-excitation cross sections.

TABLE III. Differential cross sections (a_0^2/sr) at 50 eV.

(deg)	Model	$I(0\rightarrow 0)$ $\times 10^{-2}$	$I(0\rightarrow 0)^a$ $\times 10^{-2}$	$I(0\rightarrow 2)$ $\times 10^{-2}$	$I(1\rightarrow 1)$ $\times 10^{-2}$	$I(1\rightarrow 1)^a$ $\times 10^{-2}$	$I(1\rightarrow 3)$ $\times 10^{-2}$	$\langle I\rangle$ $\times 10^{-2}$	$\langle I\rangle^a$ $\times 10^{-2}$
0	A	1301	1453	0.523	1301	1453	0.347	1301	1453
	B	1334	1504	0.764	1334	1505	0.505	1335	1506
10	A	679.3	790.7	1.933	680.1	791.5	1.192	681.3	792.7
	B	674.4	796.2	3.052	675.6	797.5	1.877	677.5	799.4
20	A	360.3	433.2	1.772	361.0	433.9	1.094	362.2	435.1
	B	329.0	405.7	3.941	330.6	407.3	2.408	333.1	409.7
30	A	194.1	238.1	1.870	194.9	238.8	1.151	196.1	240.0
	B	158.8	203.1	4.673	160.7	204.9	1.284	163.6	207.7
40	A	105.2	130.5	2.131	106.1	131.4	1.305	107.4	132.7
	B	76.92	101.3	5.014	78.93	103.2	3.045	82.02	106.2
50	A	57.59	72.16	2.449	58.57	73.09	1.493	60.10	74.65
	B	38.25	51.66	4.975	40.24	53.55	3.018	43.30	56.68
60	A	32.12	40.72	2.699	33.20	41.75	1.640	34.87	43.43
	B	19.92	27.51	4.649	21.78	29.30	2.819	24.64	32.17
70	A	18.35	23.66	2.865	19.50	24.76	1.738	21.26	26.54
	B	10.91	15.39	4.239	12.60	17.03	2.570	15.21	19.56
80	A	10.78	14.21	2.949	11.95	15.34	1.786	13.77	17.18
	B	6.244	9.006	3.854	7.785	10.51	2.335	10.15	12.86
90	A	6.527	8.846	2.941	7.703	9.980	1.780	9.503	11.79
	B	3.711	5.477	3.500	5.110	6.857	2.121	7.261	8.976
100	A	4.083	5.705	2.873	5.232	6.820	1.738	6.989	8.579
	B	2.275	3.445	3.200	3.554	4.718	1.939	5.521	6.672
110	A	2.647	3.820	2.773	3.756	4.903	1.677	5.450	6.596
	B	1.437	2.241	2.951	2.618	3.423	1.789	4.431	5.238
120	A	1.788	2.667	2.658	2.851	3.709	1.606	4.473	5.324
	B	0.941	1.515	2.744	2.038	2.619	1.663	3.725	4.315
140	A	0.946	1.496	2.431	1.918	2.458	1.470	3.402	3.927
	B	0.462	0.796	2.430	1.434	1.780	1.474	2.929	3.292
160	A	0.635	1.045	2.278	1.546	1.951	1.377	2.937	3.334
	B	0.293	0.530	2.248	1.192	1.442	1.364	2.576	2.845
180	A	0.554	0.924	2.222	1.443	1.810	1.343	2.799	3.161
	B	0.250	0.460	2.184	1.123	1.347	1.325	2.468	2.712

[a] With exchange. $\langle I\rangle^a$ does not include the effect of exchange on rotational-excitation cross sections.

TABLE IV. Total cross sections (πa_0^2).

Energy (eV)	Model	$\sigma(0\to0)$ $\times10^{-3}$	$\sigma(0\to0)$ [a] $\times10^{-3}$	$\sigma(0\to2)$ $\times10^{-3}$	$\sigma(1\to1)$ $\times10^{-3}$	$\sigma(1\to1)$ [a] $\times10^{-3}$	$\sigma(1\to3)$ $\times10^{-3}$	$\langle\sigma\rangle$ $\times10^{-3}$	$\langle\sigma\rangle$ [a] $\times10^{-3}$	$\langle\sigma\rangle$ [b] $\times10^{-3}$
20	A	3303	4020	71	3331	4046	44	3378	4093	4259 [g]
	B	3007	3888	142	3063	3938	88	3154	4031	
						5188 [c]		5330 [e]		
30	A	2698	3341	90	2735	3374	55	2791	3432	2558 [g]
	B	2332	3024	150	2392	3080	92	2486	3176	
						3458 [c]		3670 [e]		
40	A	2233	2752	100	2273	2790	61	2335	2852	1895 [g]
	B	1882	2408	148	1941	2466	90	2033	2556	
					2339 [d]	3142 [d]	158 [d]	2497 [d]	3300 [d]	
					1887 [c]	3015 [c]	361 [c]	2248 [c]	3376 [c]	
50	A	1890	2305	103	1931	2345	63	1995	2407	
	B	1571	1978	142	1628	2033	86	1716	2120	
								2260 [e]		
75	A	1355	1605	98	1394	1644	59	1454	1703	982 [g]
	B	1108	1343	123	1157	1392	74	1232	1466	
100	A	1054	1219	86	1088	1253	52	1141	1305	961 [h]
	B	855	1006	105	897	1048	63	960	1112	
								1160		
150	A	729	816	64	755	841	39	794	880	538 [h]
	B	587	665	77	617	695	46	664	742	
								780 [f]		
200	A[i]	411	458	47	430	477	28	458	505	388 [h]
	B	446	494	59	470	517	35	505	553	
								586 [f]		

[a] With exchange. Since the exchange potential used is spherically symmetric $\langle\sigma\rangle$ [a] does not include the effect of exchange on the rotational cross sections.

[b] Experimental.

[c] Reference 5. Entries in columns 9 and 10 are obtained using Eq. (11).

[d] Reference 6 (potential models 3 and 3XE). Entries in columns 9 and 10 are obtained using Eq. (11).

[e] Reference 20 (potential model B/P, Tables III and IV).

[f] Reference 21.

[g] Reference 15.

[h] Reference 14.

[i] Calculated with the cut-off parameter $R_0 = 2a_0$

Apart from our test calculations[1] by the present method recently there have appeared only two other theoretical calculations on the pure elastic and rotational excitation of H_2, one using the infinite-order sudden approximation at 10–40 eV by Truhlar *et al.*[5] and the other using the truncated close-coupling approximation (CCA) at 10 and 40 eV by Truhlar and Brandt.[6] At 40 eV (Fig. 1) where comparison is possible we use the cross sections of CCA which yielded better results.[6] Of the different potential models used by Truhlar and Brandt we choose for comparison their model 3 which is close to our model B. For the elastic cross section $(1\to1)$ it is found that our model B cross sections give better agreement to experiment than those of Truhlar and Brandt at intermediate scattering angles. For the inelastic process $(1\to3)$ the magnitude of CCA cross sections is higher but the angular dependence is exactly identical with that of model B cross sections. Even the maximum occurs at the same scattering angle 50°. It is also true for other potential models considered by Truhlar and Brandt. We can not explain why, in contrast with other potential models used in different approximations, the potential model A give proper shape of the inelastic $(1\to3)$ differential cross section at 40 eV. The polarization potential in the form taken in model A is known to account for a part of the electron-exchange effect. Test calculations with cutoff parameter less than $1.6a_0$ show that the change in magnitude of inelastic cross sections is not so significant but the scattering angle at which the minimum occurs decreases and the cross sections become more isotropic.

The ratio $R = I(1\to3,\theta)/I(1\to1,\theta)$ measures the relative importance of inelastic cross sections over the elastic cross sections and is interesting

TABLE V. Momentum-transfer cross sections (πa_0^2).

Energy (eV)	Model	$\sigma_m(0\to 0)$ $\times 10^{-3}$	$\sigma_m(0\to 0)$ [a] $\times 10^{-3}$	$\sigma_m(0\to 2)$ $\times 10^{-3}$	$\sigma_m(1\to 1)$ $\times 10^{-3}$	$\sigma_m(1\to 1)$ [a] $\times 10^{-3}$	$\sigma_m(1\to 3)$ $\times 10^{-3}$	$\langle\sigma_m\rangle$ $\times 10^{-3}$	$\langle\sigma_m\rangle$ [a] $\times 10^{-3}$	$\langle\sigma_m\rangle$ [b] $\times 10^{-3}$
20	A	1313	1658	76	1343	1684	47	1392	1734	2193
	B	1007	1404	140	1062	1453	86	1151	1546	
30	A	837	1091	97	876	1127	59	936	1189	1142
	B	593	837	142	649	890	87	738	979	
40	A	550	717	105	592	757	64	657	823	674
	B	376	524	134	430	576	81	512	658	
					501 [c]	658 [c]	143 [c]	644 [c]	801 [c]	
								357 [d]		
50	A	379	489	105	422	531	64	486	594	
	B	255	348	123	304	397	75	380	472	
75	A	181	225	90	217	261	54	271	315	251
	B	120	156	96	158	194	58	217	253	
100	A	105	126	70	133	154	42	175	197	
	B	69	87	73	98	116	44	143	161	
150	A	49	56	40	65	72	24	89	96	
	B	32	38	41	49	55	25	74	80	
200	A [e]	22	25	23	31	34	14	45	48	
	B	19	21	24	29	31	15	44	46	

[a] With exchange. Since the exchange potential used is spherically symmetric $\langle\sigma_m\rangle$ [a] does not include the effect of exchange on the rotational cross sections.

[b] Experimental results of Ref. 15.

[c] Reference 6 (potential models 3 and 3XE). Entries in columns 9 and 10 are obtained using Eq. (11).

[d] Reference 5.

[e] Calculated with the cut-off parameter $R_0 = 2a_0$.

experimentally because it is independent of uncertainties in absolute normalization of $I(1\to 3,\theta)$ and $I(1\to 1,\theta)$. In Fig. 4 the dependence of R on the scattering angle θ is shown at energies 20, 30, 40, and 100 eV calculated by the potential model B (without exchange) and is compared with that found experimentally[4,5] at 40 eV. At each energy the calculated R increases with θ and crosses unity at $\geq$50 eV at large scattering angles. Srivastava *et al.*[4], however found experimentally that R becomes unity at 110° even at 40 eV. It is to be noted that the ratio R will increase if we use the thermally averaged elastic cross section as defined in Ref. 6 in accordance with experimental condition, because the numerator in R will then decrease due to the fact that pure elastic cross sections decrease with the increase in J. Inclusion of exchange may further improve the agreement with experiment. Calculations with model A are similar to those of model B and we have already compared these at 40 eV with the experimental results of Srivastava *et al.* in I. Figure 4 shows that R increases with energy throught the scattering angles which is observed by Srivastava *et al.* only at large scattering angles (115°). At small scattering angle (20°) the situation is reversed. In Fig. 5 the variation of the calculated $I(1\to 3,\theta)$ with energy is shown at angles 20° and 110°. At 20° cross sections are found to increase very slowly for both the models while those for model B at 110° decrease with energy. In case of model A cross sections increase initially and then decrease showing a maximum at 50 eV. Srivastava *et al.* observed that both at the small scattering angle (20°) and large scattering angle (115°) $I(1\to 3,\theta)$ decrease with the increase in energy.

C. Average elastic differential cross sections

Average elastic differential cross sections for the two models A and B at electron energies 20–200 eV are shown in Figs. 6–9. Since our local-exchange potential is spherically symmetric these cross sections do not include the effect of exchange on rotational excitation. Comparison is made with recent experimental measurements which include the rotational-excitation cross sections. We do not consider the experimental results prior to 1969 since these were compared earlier[2] and the general conclusions regarding them remain unaltered. Measurements of Van Wingerden *et al.*[14] at 100–200 eV and 5°–50° and Srivastava *et al.*[15] at 20–75 eV and 20°–135° are absolute, while those of Fink *et al.*,[16] the Australian group,[17] and Williams[18] at energies shown are relative. We do not normalize any of the relative measurements with our

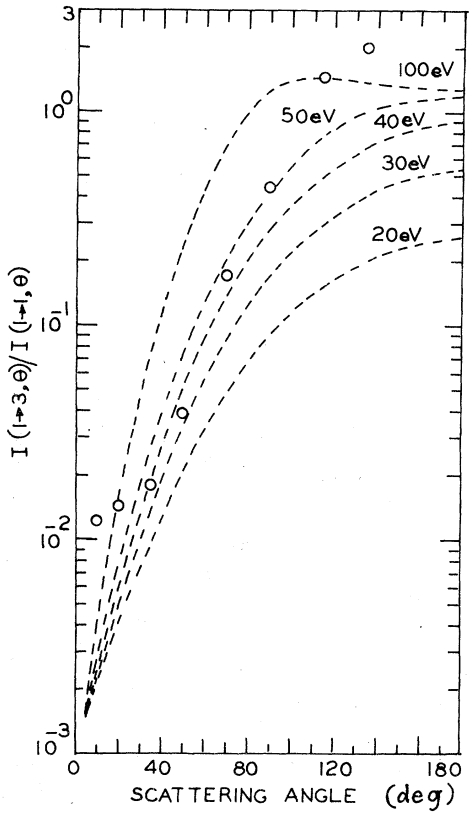

FIG. 4. Ratios of rotational-excitation cross sections for transition $J=1\rightarrow J'=3$ to elastic cross sections for transition $J=1\rightarrow J'=1$ as a function of scattering angles. Open circles are the experimental results at 40 eV of Ref. 4 as reported in Ref. 5. Broken curves are results of present calculation for potential model B (without exchange) at energies indicated.

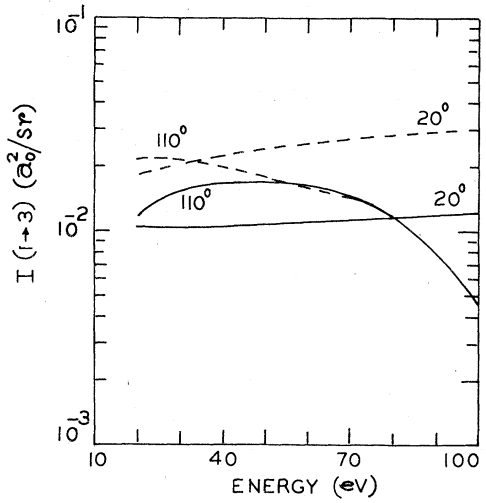

FIG. 5. Rotational-excitation cross sections for transition $J=1\rightarrow J'=3$ as a function of energy at angles 20° and 110°. Solid and broken curves are present results (without exchange) for potential models A and B, respectively.

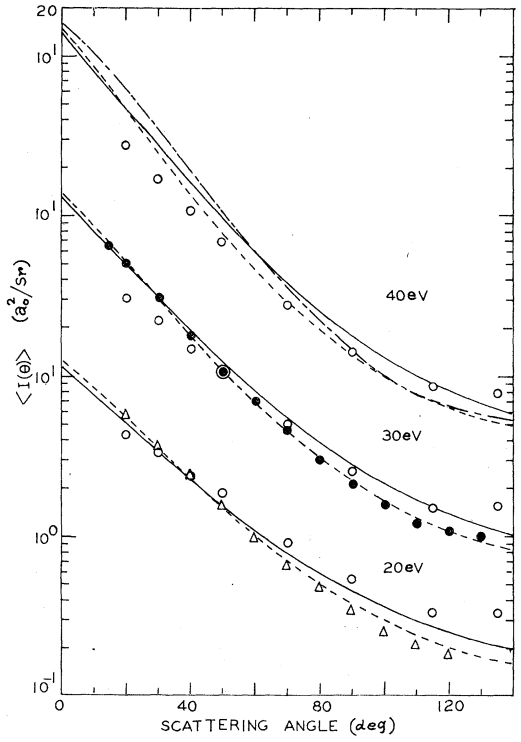

FIG. 6. Average differential cross sections at energies 20, 30, and 40 eV. Experimental: ○, Ref. 15; △ and ●, Ref. 17. Theoretical: straight line, model A and dashed line, model B, present results; dash-dotted line, Ref. 6 (these results are obtained by using Eq. (10) in which their models 3 and 3XE cross sections are used for transitions $J=1\rightarrow J'=1$ and $J=1\rightarrow J'=3$, respectively).

calculated cross sections. We use tabulated values of these measurements at 100 and 200 eV as reported in Ref. 14. At 40 and 75 eV, and 150 eV the only experimental measurements available are those of Srivastava *et al.* and Van Wingerden *et al.*, respectively.

Measurement of Srivastava *et al.* at 20–40 and 75 eV (Figs. 6 and 7) underestimate our calculations considerably at small-scattering angles and overestimate them at large angles, but they agree well in the intermediate angles. However we find excellent agreement throughout the angular region with the measurements of the Australian group at 20, 30, and 50 eV. Figure 8 shows that our cross sections at 100 eV are in very good agreement at all angles with those of different experimental workers.[14,16-18] At small angles the agreement is better with the measurements of Van Wingerden *et al.* and Fink *et al.* This is true also at 150 and 200 eV, although the magnitude of the calculated

cross sections are slightly higher (Figs. 8 and 9). At these energies however our results deviate significantly at large-scattering angles. In essence we observe that the angular dependence as well as magnitude of our calculated cross sections, particularly the model B cross sections, at energies 20–100 eV give very good fit to those obtained experimentally by different workers with the exception of Srivastava *et al.* They differ only at large-scattering angles (>90°) at higher energies (150 and 200 eV).

Figures 6–9 show some general trend of the angular dependence of average differential cross sections calculated on the basis of models A and B. At every energy model B curve is always steeper at small-scattering angles and falls below the corresponding model A curve at an angle which depends upon the energy. At large-scattering angles the two curves tend to be identical. Considering the magnitude, shape, and the angular region covered it is the model B curve which always gives better fit to experiment. We noticed this superiority of potential model B over model A when we studied the average total scattering cross sections for positron-hydrogen molecule system.[19] Another

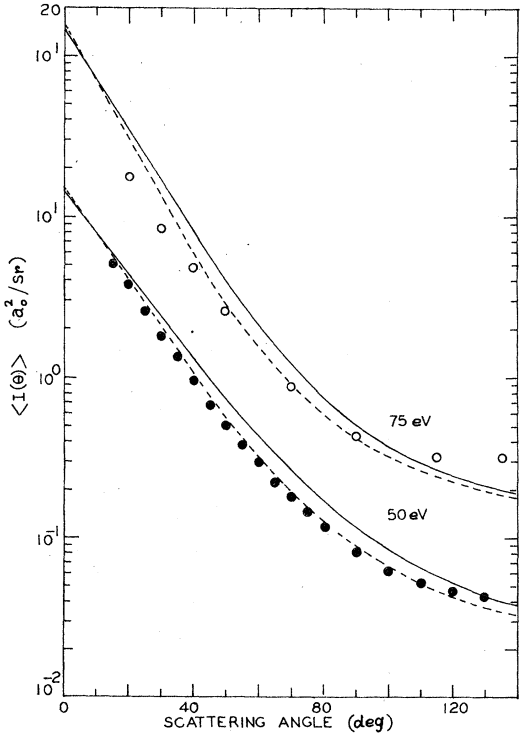

FIG. 7. Average elastic differential cross sections at energies 50 and 70 eV. Experimental: ○, Ref. 15; ●, Ref. 17. Theoretical: straight line, model A and dashed line, model B, present results.

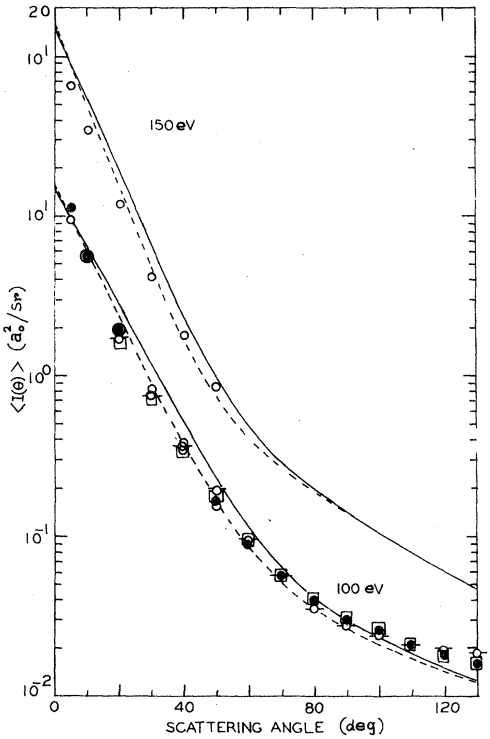

FIG. 8. Average elastic differential cross sections at energies 100 and 150 eV. Experimental: ○, Ref. 14; ●, Ref. 16; ⊖, Ref. 17; □, Ref. 18 (results of the last three measurements are given in tabular form in Ref. 14). Theoretical: straight line, model A and dashed line, model B, present results.

important difference between the two models is that the rise of forward scattering cross section with energy is greater in case of model A. At 200 eV we use the cutoff parameter $R_0 = 2a_0$ for potential model A. Comparison of our previous[2] (not shown in the figures) and present calculations with exchange at large scattering angles for model A at 30, 50, and 100 eV shows that the latter is very close to experiments. It indicates that the averaging procedure employed earlier is not proper at these and still higher energies. Test calculations below 20 eV with electrons as projectiles give almost identical cross sections using both the method of averaging. It confirms our previous conclusion[2] that nonspherical potential does not influence very much the average cross sections at lower energies. The inherent shortcoming of the Glauber-type eikonal approximation due to the neglect of longitudinal momentum transfer is the reason for the deviations observed at high-energy large-angle scattering cross sections. In case of e^--H_2 scattering it begins to show up appreciably at energies above 100 eV. To study the effect of exchange,

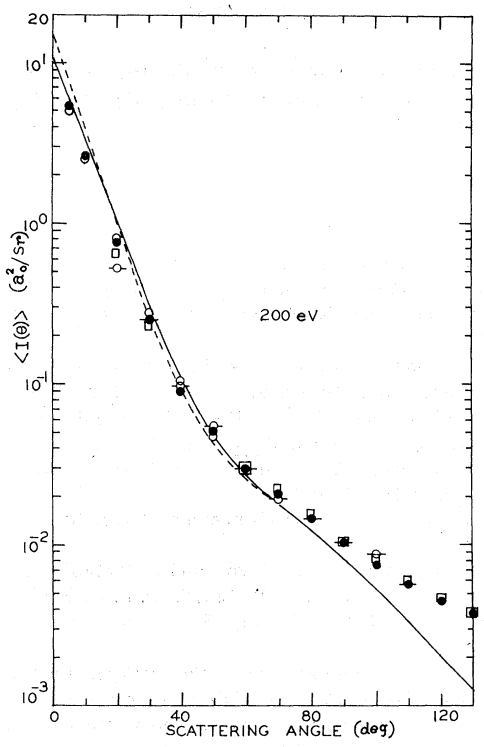

FIG. 9. Average elastic differential cross sections at energy 200 eV. Notations used are the same as in Fig. 8. Model A results are obtained with cutoff parameter $R_0 = 2a_0$.

average differential cross sections are calculated for both the models with the exclusion of the exchange term at all energies reported here. We observe no significant difference between the two models and influence of exchange on cross sections is similar to that we found earlier.[2] To avoid confusion in graphs cross sections without exchange are not plotted but are given for energies 30, 40, and 50 eV in Tables I–III (columns 9 and 10) to show the effect of exchange in general.

Only a few previous theoretical calculations on average elastic scattering of intermediate energy electrons by hydrogen molecule exist in the literature. We reviewed and compared the results of these calculations earlier[2] with those of our model A calculations. For the sake of clarity in graphs and to avoid repeatation we do not consider them in the present article although the conclusions drawn in the previous study remain unaltered. In Fig. 6, however, the recent theoretical cross sections at electron energy 40 eV obtained by Truhlar and Brandt[6] are compared with those of our present calculations. Truhlar and Brandt's cross sections shown in the graph are obtained by using Eq. (10) in which their model 3 and 3XE cross sections are used for transitions $J=1 \rightarrow J'=1$ and $J=1 \rightarrow J'=3$, respectively. We find that our calculations yield better agreement with experiment at small and intermediate scattering angles.

D. Total and momentum transfer cross sections

In Table IV total cross sections for different pure elastic and inelastic processes and average total cross sections [calculated using Eqs. (8) and (9)] at energies 20–200 eV are given to compare their relative magnitudes. Different momentum-transfer cross sections are shown in Table V. It is evident from Tables IV and V that average total and momentum-transfer cross sections are independent of the initial rotational state of the molecule (see Sec. IV B). Experimental average total cross sections of Srivastava *et al.*[15] at 20–40, 75 eV and Van Wingerden *et al.*[14] at 100–200 eV (column 11, Table IV) and experimental momentum-transfer cross sections of Srivastava *et al.*[15] at 20–40, 75 eV (column 11, Table V) are found to be in reasonably good agreement with our corresponding theoretical cross sections. The agreement is better with potential model B calculations. Finally, theoretical average total cross sections (neglecting exchange) of Trajmar *et al.*[20] and Truhlar and Rice[21] and total and momentum-transfer cross sections of Truhlar *et al.*[5] and Truhlar and Brandt[6] at energies shown in Tables IV and V are compared with those of our present calculations. We find that the average total cross sections obtained by us give better agreement with the experiment than those calculated by these workers.

V. CONCLUSIONS

In the present investigation we find that the Glauber-type eikonal amplitude predicts pure and average elastic (differential as well as total) cross sections which are very close to experimental values. For differential cross sections the agreement is very good both in shape and in magnitudes, particularly at small-scattering angles. The predicted pure rotational excitation cross sections are somewhat less in magnitude; the characteristic features of these cross sections are however in qualitative agreement with those obtained experimentally or theoretically using different methods by other workers. Of the two long-range potential models considered here the potential model B give better agreement with experimental observations. The potential model A is superior to model B only

in reproducing the angular dependence of pure inelastic differential cross sections.

In essence we observe that the problem of electron–hydrogen-molecule scattering can adequately be explained using Glauber-type eikonal amplitude.

ACKNOWLEDGMENT

This work was supported by the Indian Space Research Organization under Project No. 10/2(1)/76-III.

---

*On leave of absence from Department of Theoretical Physics, Indian Association for the Cultivation of Science, Calcutta 700 032, India.

[1]P. K. Bhattacharyya and A. S. Ghosh, Phys. Rev. A 14, 1587 (1976). This paper will be referred to as I.

[2]P. K. Bhattacharyya and A. S. Ghosh, Phys. Rev. A 12, 480 (1975). The coefficient of the first term of $V_s^2(r_3)$ for $r_3 \leq 0.7a_0$ in Eq. (6) of this paper should read -5.01637.

[3]K. Takayanagi and Y. Itikawa, in *Advances in Atomic and Molecular Physics*, edited by D. R. Bates and I. Esterman (Academic, New York, 1970), Vol. 6, p. 105; D. E. Golden, N. F. Lane, A. Temkin, and E. Gerjuoy, Rev. Mod. Phys. 43, 642 (1971).

[4]S. K. Srivastava, R. I. Hall, S. Trajmar, and A. Chutjian, Phys. Rev. A 12, 1399 (1975).

[5]D. G. Truhlar, R. E. Poling, and M. A. Brandt, J. Chem. Phys. 64, 826 (1976). Experimental cross sections $I(1 \rightarrow 1, \theta)$, $I(1 \rightarrow 3, \theta)$, and the ratio $I(1 \rightarrow 3, \theta)/I(1 \rightarrow 1, \theta)$ at 40 eV of Ref. 4 are given here in tabular form.

[6]D. G. Truhlar and M. A. Brandt, J. Chem. Phys. 65, 3092 (1976).

[7]K. K. Goswami, P. K. Bhattacharyya, and A. S Ghosh (unpublished).

[8]This equation should replace the Eq. (10) in I which has some misprints.

[9]S. C. Wang, Phys. Rev. 31, 579 (1928).

[10]S. Hara, J. Phys. Soc. Jpn. 22, 710 (1967).

[11]R. J. W. Henry and N. F. Lane, Phys. Rev. 183, 221 (1969).

[12]J. N. Gau and J. Macek, Phys. Rev. A 10, 522 (1974).

[13]N. F. Lane and S. Geltman, Phys. Rev. 160, 53 (1967).

[14]B. Van Wingerden, F. J. de Heer, E. Weigold, and K. J. Nygaard, J. Phys. B 10, 1345 (1977).

[15]S. K. Srivastava, A. Chutjian and S. Trajmar, J. Chem. Phys. 63, 2659 (1975).

[16]M. Fink, K. Jost, and D Herrmann, Phys. Rev. A 12, 1374 (1975).

[17]P. J. O. Teubner, C. R. Lloyd, and E. Weigold, Phys. Rev. A 9, 2552 (1974); C. R. Lloyd, P. J. O. Teubner, E. Weigold, and B. R. Lewis, Phys. Rev. A 9, 175 (1974).

[18]K. Williams, in *Proceedings of the Sixth International Conference on the Physics of Electronic and Atomic Collisions, Cambridge, Massachusetts*, 1969 (M. I. T., Cambridge, Mass., 1969), pp. 735–737.

[19]P. K. Bhattacharyya and A. S. Ghosh, Phys. Rev. A 12, 1881 (1975).

[20]S. Trajmar, D. G Truhlar, and J. K. Rice, J. Chem. Phys. 52, 4502 (1970).

[21]D. G. Truhlar and J. K. Rice, J. Chem. Phys. 52, 4480 (1970).